

# Part to Whole: Collaborative Prompting for Surgical Instrument Segmentation

Wenxi Yue<sup>1</sup>, Jing Zhang<sup>1</sup>, Kun Hu<sup>1</sup>, Qiuxia Wu<sup>2</sup>, Zongyuan Ge<sup>3</sup>, Yong Xia<sup>4</sup>, Jiebo Luo<sup>5</sup>, Zhiyong Wang<sup>1</sup>

<sup>1</sup>School of Computer Science, The University of Sydney

<sup>2</sup>School of Software Engineering, South China University of Technology

<sup>3</sup>Department of Data Science & AI, Monash University

<sup>4</sup>School of Computer Science, Northwestern Polytechnical University

<sup>5</sup>Department of Computer Science, University of Rochester

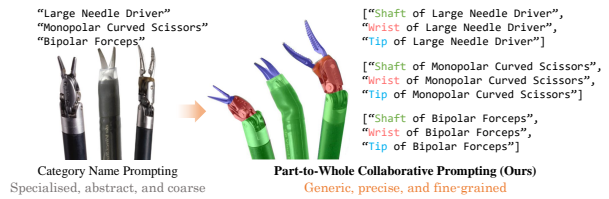
{wenxi.yue, jing.zhang1, kun.hu, zhiyong.wang}@sydney.edu.au, qxwu@scut.edu.cn, Zongyuan.Ge@monash.edu, yxia@nwpu.edu.cn, jluo@cs.rochester.edu

## Abstract

Foundation models like the Segment Anything Model (SAM) have demonstrated promise in generic object segmentation. However, directly applying SAM to surgical instrument segmentation presents key challenges. First, SAM relies on per-frame point-or-box prompts which complicate surgeon-computer interaction. Also, SAM yields suboptimal performance on segmenting surgical instruments, owing to insufficient surgical data in its pre-training as well as the complex structure and fine-grained details of various surgical instruments. To address these challenges, in this paper, we investigate text promptable surgical instrument segmentation and propose SP-SAM (SurgicalPart-SAM), a novel efficient-tuning approach that integrates surgical instrument structure knowledge with the generic segmentation knowledge of SAM. Specifically, we achieve this by proposing (1) collaborative prompts in the text form “[part name] of [instrument category name]” that decompose instruments into fine-grained parts; (2) a Cross-Modal Prompt Encoder that encodes text prompts jointly with visual embeddings into discriminative part-level representations; and (3) a Part-to-Whole Selective Fusion and a Hierarchical Decoding strategy that selectively assemble the part-level representations into a whole for accurate instrument segmentation. Built upon them, SP-SAM acquires a better capability to comprehend surgical instrument structures and distinguish between various categories. Extensive experiments on both the EndoVis2018 and EndoVis2017 datasets demonstrate SP-SAM’s state-of-the-art performance with minimal tunable parameters. Code is at <https://github.com/wenxi-yue/SurgicalPart-SAM>.

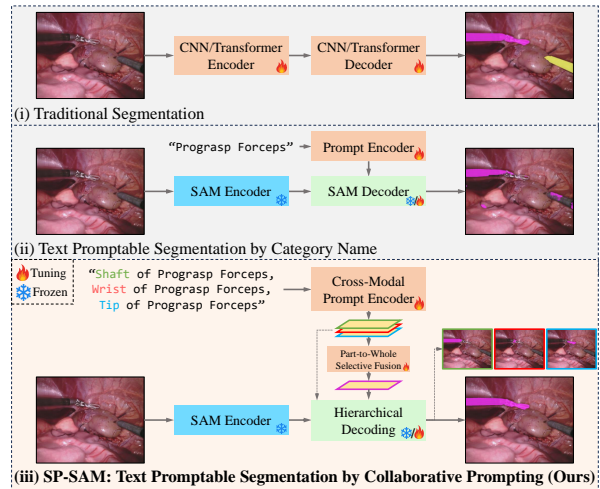
## 1. Introduction

Surgical instrument segmentation aims to accurately identify and delineate surgical instruments in operative scenes.



Category Name Prompting: Specialised, abstract, and coarse  
Part-to-Whole Collaborative Prompting (Ours): Generic, precise, and fine-grained

(a) Category Name Prompts vs Collaborative Prompts (Ours).



(b) Comparison of the proposed SP-SAM with traditional segmentation and segmentation prompted by category name.

Figure 1. SP-SAM with collaborative prompts incorporates the knowledge of surgical instrument structures and guides attention towards their intricate details.

It plays a foundational role for many downstream applications, such as surgical planning [7], robotic navigation [43], and skill assessment [24]. We identify two primary problems with the existing methods for this task. First, they often develop specialist models that require full training of all parameters (Fig. 1b-(i)), leading to high development costs. Second, current methods lack the capability of human-computer interaction that is highly desired in surgi-

cal practice [4, 6].

The Segment Anything Model (SAM) [22] is a pioneering foundation model for promptable segmentation. It holds great potential for addressing the above problems owing to its rich pre-trained knowledge and interactivity. However, there still exist some fundamental challenges that impede the application of SAM in surgical instrument segmentation. Firstly, SAM’s reliance on point-or-box prompts is impractical in surgical settings, where it is infeasible for surgeons to provide such prompts for every instrument in each frame. Instead, more flexible and efficient prompts like free-form text would be preferred (*e.g.*, via speech recognition and voice control). Secondly, SAM has shown subpar zero-shot generalisation in segmenting surgical instruments [42] due to insufficient surgical data in pre-training as well as the complex structure and fine-grained nature of surgical instruments across various categories.

In this paper, we investigate text promptable surgical instrument segmentation and propose a novel framework, SP-SAM (SurgicalPart-SAM), that addresses the above challenges by leveraging SAM’s generic segmentation capability while integrating instrument structure information via an efficient model tuning scheme (Fig. 1b-(iii)). For text-prompted segmentation, a common practice is to use the object names to prompt the segmentation of an object of interest. However, the category names of instruments are not ideal for use as text prompts due to their specialised and abstract nature (Fig. 1a and Fig. 1b-(ii)). To this end, we introduce a new form of text prompt, namely Collaborative Prompt, using a text description set:  $\{“[part\ name]\ of\ [instrument\ category\ name]”\}$  for all parts of an instrument category. It combines both category and part information, effectively decomposing the specialised, abstract, and coarse concepts of instrument categories into more precise and fine-grained instrument parts, which is more appropriate for surgical instruments of high structure complexity (Fig. 1a and Fig. 1b-(iii)).

To encode these collaborative prompts, we introduce a Cross-Modal Prompt Encoder, transforming collaborative prompts into part-level sparse and dense prompt embeddings for SAM’s mask decoder through visual-textual interaction. This enables focused learning of fine-grained representations for each instrument part, enhancing segmentation of subtle details. Finally, to integrate the knowledge of instrument structure into the model, a Part-to-Whole Selective Fusion and a Hierarchical Decoding strategy are proposed. Specifically, we adaptively assemble the learned part-level sparse and dense embeddings considering both category-specific and image-specific part weights, to predict the mask of the whole instrument. Afterwards, hierarchical decoding of both the whole instrument and its parts is performed to enhance the understanding of surgical instruments both holistically and at the part level.

To this end, SP-SAM has strong capability to comprehend surgical instrument structures, identify subtle details, and discriminate between fine-grained categories. In summary, our contributions are three-fold:

- We introduce a novel approach SP-SAM for text promptable surgical instrument segmentation, offering a simpler prompting pipeline than the vanilla SAM that better suits the demands of surgical practices. SP-SAM achieves state-of-the-art (SOTA) performance on the challenging EndoVis2018 and EndoVis2017 datasets while requiring only a small number of training parameters.
- We introduce a new type of text prompt integrated with both instrument category and part information, namely collaborative prompts, and devise a Cross-Modal Prompt Encoder, which encodes text prompts jointly with visual embeddings into discriminative part-level representations, ensuring accurate segmentation of subtle details.
- We propose a Part-to-Whole Selective Fusion and a Hierarchical Decoding strategy to adaptively assemble the part-level representations into a whole and make predictions at both the part-level and the holistic-level, explicitly incorporating structure information regarding category-part relations and achieving better discrimination between categories.

## 2. Related Work

### 2.1. Surgical Instrument Segmentation

Most surgical instrument segmentation methods focus on developing vision-based specialist models. Early research adopts a semantic segmentation pipeline with the pioneering work TeraNet introducing a U-Net based encoder-decoder model [32]. Subsequent developments include feature pyramid attention [29] and flow-based temporal priors [20, 46]. An alternative strategy to semantic segmentation is instance segmentation. ISINet adopts Mask-RCNN [15, 16] for this task, which is later enhanced by Baby et al. [5] with a specialised classification module. In addition, TraSeTR utilises a track-to-segment transformer with tracking cues [47] and MATIS employs Mask2Former with a temporal consistency module [3, 9]. Despite the variety of the methods developed for surgical instrument segmentation, they primarily rely on developing specialist models and training the complete set of model parameters, which incurs high development costs. Furthermore, these methods predict the masks of all the instruments in a given image and lack interactivity, preventing surgeons from specifying objects of interest, a crucial aspect in surgical applications [4, 6].

Recently, surgical instrument segmentation has been formulated as a promptable task. Zhou et al. [48] introduces a text promptable framework exploiting the pre-trained vision-language model CLIP [30]. However, this approach requires complete fine-tuning of the CLIP image encoder,

leading to high computational cost. By contrast, SurgicalSAM offers an efficient-tuning approach based on SAM [42]. However, it is prompted by category IDs, which lacks flexibility and fails to leverage the rich information from both vision and text modalities.

## 2.2. Text Promptable Segmentation

In contrast to traditional segmentation that solely relies on pre-defined class labels, text promptable segmentation uses natural language as prompts that can offer richer contextual information, improved generalisation, and greater flexibility. Early works are primarily based on convolutional neural networks and recurrent neural networks and propose attention mechanisms for extracting and relating visual and textual features [18, 23, 31, 41]. More recent approaches utilise transformers to perform feature extraction and multi-modal feature fusion [12, 14, 21, 36, 40]. Recently, to leverage the rich knowledge of large-scale pre-training, large vision-language models such as CLIP [30] are utilised for this task [25, 35]. However, these methods, primarily designed for natural objects, are not specifically tailored to the unique and distinct challenges presented by surgical instruments.

## 2.3. Segment Anything Model

SAM is recognised as the pioneering foundation model for image segmentation. Owing to extensive pre-training on large-scale data, SAM exhibits impressive generalisation capabilities on various downstream tasks [22]. However, its zero-shot performance in medical contexts tends to fall short due to the significant disparity between natural and medical subjects [10, 11, 17, 19, 27, 42]. Moreover, SAM’s reliance on precise per-frame point-or-box prompts for segmentation [10, 33] requires extensive manual input, infeasible in many medical scenarios, *e.g.* during surgery. To mitigate the gap between natural and medical domains, some studies have fine-tuned SAM with domain-specific data. However, these methods either have limited interactivity [8, 34, 44], require labour-intensive per-frame points or bounding boxes for prompting [26, 37], or rely solely on pre-defined category IDs [42]. While prompts in the form of text are highly desired, there is limited research on the application of SAM with text prompts.

## 3. Method

In this paper, we address the task of text promptable surgical instrument segmentation. Instrument category names are not ideal for use as text prompts due to their specialised, abstract, and coarse nature. Therefore, we introduce collaborative text prompts that combine both category and part information of surgical instruments. To maximise the potential of these collaborative prompts and integrate instrument structure information with SAM’s generic knowledge, we propose a part-to-whole collaborative prompting pipeline

based on SAM, namely SP-SAM. Given a surgical image  $I \in \mathbb{R}^{H \times W \times 3}$  of size  $H \times W$  and collaborative text prompts  $T^{(c)}$  for an instrument category  $c$ , SP-SAM predicts the binary mask  $M^{(c)} \in \{0, 1\}^{H \times W}$  for the instrument.

With the collaborative prompts, instrument structure information can be easily integrated by establishing a category-part relation matrix  $\mathcal{D}_{CP} \in \{0, 1\}^{C \times P}$ , where  $C$  and  $P$  denote the numbers of surgical instrument categories and instrument parts, respectively, and each element  $d_{cp}$  in  $\mathcal{D}_{CP}$  indicates the presence of part  $p$  in category  $c$ . For instance, monopolar curved scissors (the middle tool in Fig. 1a), composed of shaft and tip parts, would have 1s for these parts and 0s for absent parts like the wrist. SP-SAM leverages the instrument structure priors  $\mathcal{D}_{CP}$  for accurate surgical segmentation.

As shown in Fig. 2, SP-SAM consists of four key components: (1) a frozen SAM Image Encoder that extracts image embeddings from the given image, (2) a Cross-Modal Prompt Encoder (Sec. 3.1) that extracts part embeddings from collaborative prompts and generates part sparse and dense embeddings through cross-modal interaction, (3) a Part-to-Whole Selective Fusion module (Sec. 3.2) that combines part sparse and dense embeddings into whole sparse and dense embeddings through Category Part Attention and Image Part Attention, considering category-specific and image-specific part contributions, respectively, and (4) a SAM Decoder for Hierarchical Decoding (Sec. 3.3) that decodes these embeddings into masks, thereby enhancing the model’s comprehension of instruments both as a whole and at the part level.

### 3.1. Cross-Modal Prompt Encoder

The Cross-Modal Prompt Encoder takes the collaborative prompts and image embedding as input and performs cross-modal interaction between them via spatial attention, generating part sparse embeddings and part dense embeddings. As shown in Fig. 3, this process can be divided into two steps: Feature Extraction of Collaborative Prompts and Part-Level Cross-Modal Encoding.

**Feature Extraction of Collaborative Prompts.** We introduce a new type of text prompt for surgical instruments that collaboratively integrates both category and part information, namely collaborative prompts. Specifically, the collaborative prompts for an instrument of category  $c$  are formulated into a set of texts containing all  $P$  parts:  $T^{(c)} = \{[part_p] \text{ of } [instrument\ category_c]\}_{p=1}^P$ , where *instrument category<sub>c</sub>* and *part<sub>p</sub>* represent the names in text for instrument category  $c$  and part  $p$ , respectively. Next,  $T^{(c)}$  is encoded by the CLIP Text Encoder [30] into text-based CLIP part embeddings  $\mathcal{T}_{clip}^{part} \in \mathbb{R}^{P \times d_{clip}}$ . A challenge here is the inherent distribution mismatch between the embedding spaces of SAM and CLIP. To transfer the CLIP

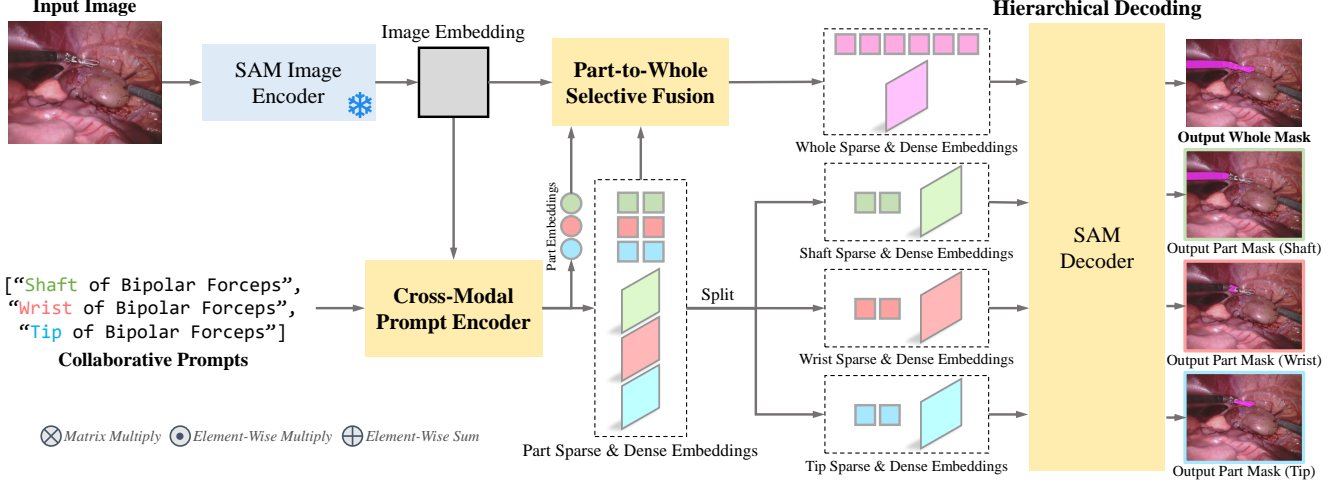


Figure 2. **Overview of the proposed SP-SAM.** SP-SAM consists of four main components: a SAM Image Encoder, a Cross-Modal Prompt Encoder, a Part-to-Whole Selective Fusion module, and a SAM Decoder. The SAM Image Encoder and CLIP Text Encoder (within the Cross-Modal Prompt Encoder) are frozen and the remaining weights are tuned. SP-SAM achieves text promptable surgical instrument segmentation through collaborative prompting, part-to-whole selective fusion, and hierarchical decoding.

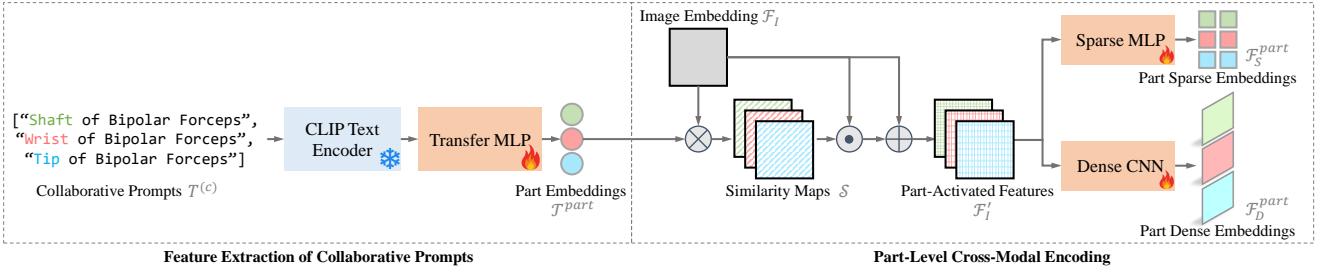


Figure 3. **Cross-Modal Prompt Encoder** consists of Feature Extraction of Collaborative Prompts and Part-Level Cross-Modal Encoding.

text embeddings into SAM’s embedding space, a tunable Transfer MLP is devised and applied to  $\mathcal{T}_{clip}^{part}$ , leading to the transferred embeddings for the parts, namely part embeddings  $\mathcal{T}^{part} \in \mathbb{R}^{P \times d}$ , where  $d$  matches the number of embedding channels of SAM’s image features.

**Part-Level Cross-Modal Encoding.** In this step, the part embeddings  $\mathcal{T}^{part}$  interact with the image embedding via spatial attention, and the obtained part-activated features are used to generate part sparse and dense embeddings. Specifically, the SAM Image Encoder extracts the image embedding  $\mathcal{F}_I \in \mathbb{R}^{h \times w \times d}$ , where  $h \times w$  is the feature size. We then design a spatial attention mechanism by computing a similarity map for each part, leading to  $\mathcal{S} = \mathcal{T}^{part} \times \mathcal{F}_I^T \in \mathbb{R}^{P \times h \times w}$ , where  $\top$  denotes a transpose operator. These similarity maps serve as part-aware spatial attention to activate the image embedding, augmenting  $\mathcal{F}_I$  into  $\mathcal{F}_I^part = \mathcal{S} \circ \mathcal{F}_I + \mathcal{F}_I \in \mathbb{R}^{P \times h \times w \times d}$ , where  $\mathcal{F}_I$  and  $\mathcal{S}$  are broadcasted to the same size and  $\circ$  denotes the Hadamard product. The part-activated features  $\mathcal{F}_I^part$ , containing infor-

mation of both the image and the collaborative prompts, are used to compute part sparse embeddings  $\mathcal{F}_S^{part} \in \mathbb{R}^{P \times n \times d}$  and part dense embeddings  $\mathcal{F}_D^{part} \in \mathbb{R}^{P \times h \times w \times d}$  with a two-layer MLP and a three-layer CNN, respectively. Here  $n$  represents the number of sparse tokens for each part. These embeddings are then fed into the SAM Decoder to segment the corresponding instrument parts.

### 3.2. Part-to-Whole Selective Fusion

In the Part-to-Whole Selective Fusion module, the sparse and dense embeddings for all parts are selectively fused to form the whole sparse and dense embeddings,  $\{\mathcal{F}_S, \mathcal{F}_D\}$ , for the segmentation of the entire instrument. The selective fusion is achieved through Category Part Attention and Image Part Attention, as shown in Fig. 4.

Specifically, the part sparse and dense embeddings consist of the prompt embeddings of all  $P$  parts. However, as established in  $\mathcal{D}_{CP}$ , instruments of a category encompass only a subset of these parts. Therefore, we propose a Category Part Attention that utilises the part weights for

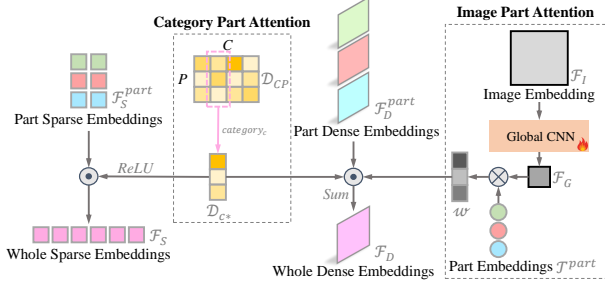


Figure 4. **Part-to-Whole Selective Fusion Module** assembles part sparse and dense embeddings into whole sparse and dense embeddings via Category Part Attention and Image Part Attention.

the prompted category  $c$  in  $\mathcal{D}_{CP}$ , i.e.,  $\mathcal{D}_{c^*} = \{d_{cp}\}_{p=1}^P \in \mathbb{R}^{1 \times P}$ , as the weights to fuse the sparse and dense embeddings from the part level to the whole level. Note that  $\mathcal{D}_{CP}$  is initialised with 0s and 1s but is updated dynamically during model training.

While the Category Part Attention provides category-specific part weights based on expert knowledge, the presence and contribution of each part to an instrument can vary significantly across images due to different field-of-views and occlusions. Therefore, it is necessary to adapt the part-to-whole fusion to the condition of each image. Accordingly, we propose Image Part Attention to compute image-specific part weights by learning a global descriptor of the image and computing its similarity with the part embeddings. Particularly, the global descriptor  $\mathcal{F}_G \in \mathbb{R}^{1 \times d}$  is learned from image embedding  $\mathcal{F}_I$  with a Global CNN that consists of three convolutional layers and a linear layer. Then, image-specific part weights are computed as:  $\mathcal{W} = \mathcal{F}_G \times \mathcal{T}^{part\top} \in \mathbb{R}^{1 \times P}$ .

Finally, given category-specific part weights  $\mathcal{D}_{c^*}$  and image-specific part weights  $\mathcal{W}$ , we fuse the sparse and dense embeddings  $\{\mathcal{F}_S^{part}, \mathcal{F}_D^{part}\}$  of the parts into the sparse and dense embeddings  $\{\mathcal{F}_S, \mathcal{F}_D\}$  of the whole instrument as below. Note that the matrices are all broadcasted to the same size prior to the Hadamard product.

$$\mathcal{F}_S = \mathcal{F}_S^{part} \circ \text{ReLU}(\mathcal{D}_{c^*}) \in \mathbb{R}^{P \times n \times d}, \quad (1)$$

$$\mathcal{F}'_D = \mathcal{F}_D^{part} \circ \mathcal{D}_{c^*} \circ \mathcal{W} \in \mathbb{R}^{P \times h \times w \times d}, \quad (2)$$

$$\mathcal{F}_D = \sum_{p=1}^P \mathcal{F}'_D \in \mathbb{R}^{h \times w \times d}. \quad (3)$$

### 3.3. Hierarchical Decoding

The sparse and dense embeddings at both the whole level and the part level are fed into SAM Decoder for hierarchical decoding. This explicitly directs the model to learn both the overall characteristics as well as the part structures of surgical instruments. The final loss function thus comprises of the dice losses  $\mathcal{L}_D$  [28] for both the whole segmentation

mask and the part segmentation masks:

$$\mathcal{L} = \mathcal{L}_D(M^{(c)}, G^{(c)}) + \sum_{p=1}^P d_{cp} \mathcal{L}_D(M_p^{(c)}, G_p^{(c)}), \quad (4)$$

$$\mathcal{L}_D(M, G) = \frac{2 \sum_i^{HW} m_i g_i}{\sum_i^{HW} m_i^2 + \sum_i^{HW} g_i^2}, \quad (5)$$

where  $m_i$  and  $g_i$  denote the predicted logit value and the ground truth binary value at pixel  $i$ , respectively.  $M^{(c)}$  and  $\{M_p^{(c)}\}_{p=1}^P$  are the predicted masks of the instrument and its parts, respectively.  $G^{(c)}$  and  $\{G_p^{(c)}\}_{p=1}^P$  are the ground truth masks of the instrument and its parts, respectively.

## 4. Experiments

### 4.1. Datasets and Evaluation Metrics

The effectiveness of SP-SAM is validated using the EndoVis2018 [2] and EndoVis2017 [1] datasets. We follow the standard experiment and evaluation protocols defined in [32] and [15] to ensure a fair comparison with existing methods. EndoVis2018 is composed of 11 training videos and four validation videos each with 149 frames. EndoVis2017 contains eight videos each with 255 frames, where we perform 4-fold cross-validation following [32]. EndoVis2018 and EndoVis2017 offer annotations for five and four instrument parts, respectively, and both datasets include seven instrument categories.

We adopt three metrics in evaluation: Challenge IoU [1], IoU, and mean class IoU (mc IoU) [3, 5, 15]. Challenge IoU is computed only for the classes present in an image, whereas IoU considers all classes. Our promptable segmentation setting leads to identical results for Challenge IoU and IoU. Additionally, we report the IoU for each instrument category as well as their average (mc IoU).

### 4.2. Implementation Details

Images from EndoVis2017 and EndoVis2018 are processed to a size of  $1024 \times 1280$ , as per [32]. Data augmentation strategies are adopted following [3, 32], which include random flipping, random scale and crop, random rotation, and colour jitter. For Transfer MLP, Sparse MLP, Dense CNN, and Global CNN, their feature dimensions are set to 512, 256, 256, and 256, respectively. The number of sparse tokens per part  $n$  is set to 2. In terms of training, we initialise SAM Image Encoder and SAM Decoder with SAM's pre-trained weights of the ViT-H version [13]. We adopt CLIP Text Encoder of version ViT-L/14@336px, following [22]. Our model keeps SAM Image Encoder and CLIP Text Encoder frozen and updates the remaining weights using an Adam optimiser with a learning rate of 0.0001. To reduce computational load, we utilise pre-computed image embeddings, employing a batch size of 8. In practice, inspired by

Method Category	Method	Challenge IoU	IoU	mc IoU	Instrument Categories							#Params
					BF	PF	LND	SI	CA	MCS	UP	
Specialist Model	TernausNet [32]	46.22	39.87	14.19	44.20	4.67	0.00	0.00	0.00	50.44	0.00	32.20M
	MF-TAPNet [20]	67.87	39.14	24.68	69.23	6.10	11.68	14.00	0.91	70.24	0.57	37.73M
	Dual-MF [46]	70.40	-	35.09	74.10	6.80	46.00	30.10	7.60	80.90	0.10	203.80M
	ISINet [15]	73.03	70.94	40.21	73.83	48.61	30.98	37.68	0.00	88.16	2.16	162.52M
	TraSeTr [47]	76.20	-	47.71	76.30	53.30	46.50	40.60	13.90	86.20	17.15	-
	S3Net [5]	75.81	74.02	42.58	77.22	50.87	19.83	50.59	0.00	92.12	7.44	68.41M
	MATIS Frame [3]	82.37	77.01	48.65	83.35	38.82	40.19	64.49	4.32	93.18	16.17	68.72M
	TP-SIS [48]	84.92	83.61	65.44	84.28	73.18	78.88	92.20	23.73	66.67	39.12	-
SAM-based Model	MaskTrack-RCNN [39] + SAM	78.49	78.49	56.07	79.83	74.86	43.12	<b>62.88</b>	16.74	91.62	23.45	57.67M
	Mask2Former [9] + SAM	78.72	78.72	52.50	85.95	<b>82.31</b>	44.08	0.00	49.80	<b>92.17</b>	13.18	68.72M
	TrackAnything (1 Point) [38]	40.36	38.38	20.62	30.20	12.87	24.46	9.17	0.19	55.03	12.41	-
	TrackAnything (5 Points) [38]	65.72	60.88	38.60	72.90	31.07	<b>64.73</b>	10.24	12.28	61.05	17.93	-
	PerSAM [45]	49.21	49.21	34.55	51.26	34.40	46.75	16.45	15.07	52.28	25.62	-
	PerSAM [45]	52.21	52.21	37.24	57.19	36.13	53.86	14.34	25.94	54.66	18.57	2
	SurgicalSAM [42]	80.33	80.33	58.87	83.66	65.63	58.75	54.48	39.78	88.56	21.23	4.65M
	<b>SP-SAM (Ours)</b>	<b>84.24</b>	<b>84.24</b>	<b>65.71</b>	<b>87.60</b>	65.07	61.95	58.30	<b>59.96</b>	92.08	<b>34.99</b>	8.62M
	GT Centroid + SAM	60.26	60.26	63.34	44.35	65.92	30.99	87.14	69.69	80.04	65.26	-
	GT Bbox + SAM	88.04	88.04	84.23	87.10	86.81	72.23	91.21	75.91	93.08	83.24	-

Table 1. Comparative results on the EndoVis2018 dataset. #Params denotes the number of tunable parameters.

[42], we implement our model by inputting all categories into the model and differentiating the positive category (*i.e.*, the prompted category) with negative categories via the positive and negative sparse embeddings of SAM. SP-SAM is implemented using PyTorch and trained and evaluated on an Nvidia Tesla V100 16GB GPU.

### 4.3. Main Results

We compare the performance of SP-SAM against existing methods on the EndoVis2018 and EndoVis2017 datasets, detailed in Table 1 and Table 2, respectively. A visual comparison of the predictions is shown in Fig. 5. The instrument categories include *Bipolar Forceps (BF)*, *Prograsp Forceps (PF)*, *Large Needle Driver (LND)*, *Suction Instrument (SI)*, *Vessel Sealer (VS)*, *Clip Applier (CA)*, *Grasping Retractor (GR)*, *Monopolar Curved Scissors (MCS)*, and *Ultrasound Probe (UP)*. In our comparison, we divide existing methods into two categories: specialist models and SAM-based models. Notably, SP-SAM surpasses the existing efficient-tuning approaches based on SAM and delivers performance on par with fully-trained specialist models, yet at a substantially lower training cost in terms of tunable parameters.

In terms of zero-shot performance of SAM, the methods using bounding boxes as prompts (MaskTrack-RCNN [39] with SAM and Mask2Former [9] with SAM) in general outperform those using point prompts (TrackAnything [38]). However, their performances are still inferior to tuning-based methods. Additionally, they rely on a well-trained detector for bounding box prediction, resulting in a considerable increase in the number of training parameters and higher pipeline complexity. In contrast, tuning-based methods for SAM, including both SurgicalSAM [42] and SP-SAM, adopt an end-to-end efficient tuning pipeline

with minimal training parameters, boosting both training efficiency and segmentation performance.

Our method demonstrates considerable enhancement over the existing efficient-tuning approach, SurgicalSAM [42], on both datasets. It shows an improvement of 3.91 and 4.00 in terms of Challenge IoU on EndoVis2018 and EndoVis2017, respectively. Unlike SurgicalSAM, which uses only category IDs for prompting, our approach is prompted by free-form text, leveraging the extensive information in natural language expressions and pre-trained language models. Additionally, our method significantly outperforms SurgicalSAM in mean class IoU (mc IoU), by a gain of 6.84 for EndoVis2018 and 4.03 for EndoVis2017, indicating superior discrimination of instruments across different categories. This enhancement is largely attributed to our part-to-whole collaborative prompting mechanism that explicitly directs the model to identify the internal structures of instruments and concentrate on the part-level details, in contrast to SurgicalSAM which treats each instrument as a single entity.

In addition, we compare SP-SAM with two oracle scenarios that employ ground truth centroids and bounding boxes as prompts for SAM. Remarkably, SP-SAM’s performance closely approaches that of the oracle setting with ground truth bounding boxes, with only a gap of 3.80 and 2.37 in terms of Challenge IoU for EndoVis2018 and EndoVis2017, respectively, yet our method requires significantly less prompting effort without the need for manual per-frame bounding box guidance.

Finally, the performance of SP-SAM is on par with SOTA specialist models on both datasets, especially in terms of mc IoU. Despite the recent TP-SIS [48] achieving high Challenge IoU and IoU on EndoVis2017, its de-

Method Category	Method	Challenge IoU	IoU	mc IoU	BF	PF	Instrument Categories				
							LND	VS	GR	MCS	UP
Specialist Model	TernausNet [32]	35.27	12.67	10.17	13.45	12.39	20.51	5.97	1.08	1.00	16.76
	MF-TAPNet [20]	37.25	13.49	10.77	16.39	14.11	19.01	8.11	0.31	4.09	13.40
	Dual-MF [46]	45.80	-	26.40	34.40	21.50	64.30	24.10	0.80	17.90	21.80
	ISINet [15]	55.62	52.20	28.96	38.70	38.50	50.09	27.43	2.10	28.72	12.56
	TraSeTr [47]	60.40	-	32.56	45.20	56.70	55.80	38.90	11.40	31.30	18.20
	S3Net [5]	72.54	71.99	46.55	75.08	54.32	61.84	35.50	27.47	43.23	28.38
	MATIS Frame [3]	68.79	62.74	37.30	66.18	50.99	52.23	32.84	15.71	19.27	23.90
TP-SIS [48]	79.90	77.83	56.22	68.58	73.52	92.74	83.90	0.13	74.70	0.00	
SAM-based Model	Mask2Former [9] + SAM	66.21	66.21	55.26	66.84	<b>55.36</b>	83.29	73.52	26.24	36.26	45.34
	TrackAnything (1 Point) [38]	54.90	52.46	55.35	47.59	28.71	43.27	82.75	63.10	66.46	55.54
	TrackAnything (5 Points) [38]	67.41	64.50	62.97	55.42	44.46	62.43	<b>83.68</b>	62.59	67.03	<b>65.17</b>
	PerSAM [45]	42.47	42.47	41.80	53.99	25.89	50.17	52.87	24.24	47.33	38.16
	PerSAM [45]	41.90	41.90	39.78	46.21	28.22	53.12	57.98	12.76	41.19	38.99
	SurgicalSAM [42]	69.94	69.94	67.03	68.30	51.77	75.52	68.24	57.63	<b>86.95</b>	60.80
	<b>SP-SAM (Ours)</b>	<b>73.94</b>	<b>73.94</b>	<b>71.06</b>	<b>68.89</b>	53.16	<b>83.80</b>	73.20	<b>72.40</b>	84.91	61.05
	GT Centroid + SAM	44.42	44.42	54.41	63.42	36.03	22.57	54.21	75.18	70.17	59.25
	GT Bbox + SAM	76.31	76.31	81.18	89.36	73.44	67.67	90.04	87.79	94.03	65.91

Table 2. Comparative results on the EndoVis2017 Dataset.

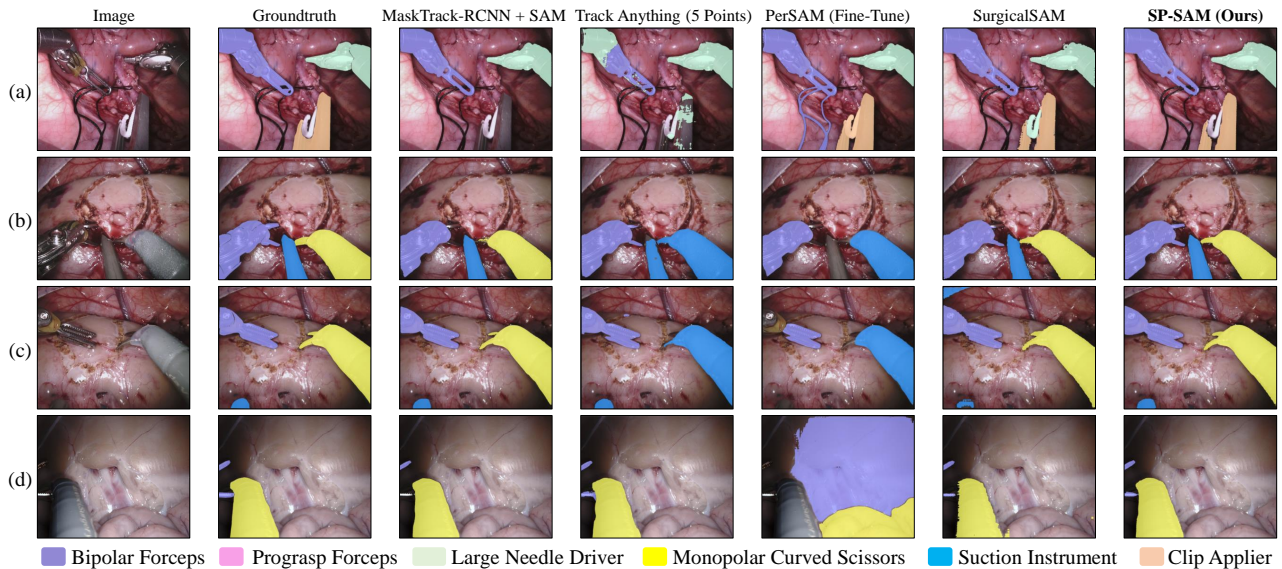


Figure 5. Visual comparison of predicted masks by different methods.

pendency on fine-tuning the entire CLIP Image Encoder makes it training-intensive. In contrast, SP-SAM offers an efficient-tuning pipeline with only 8.62M tunable parameters. This training efficiency is crucial in surgical practice, improving resource efficiency of model development and making surgical technology more affordable and adaptable to specific surgical procedures. Furthermore, by harnessing part-level structure knowledge, SP-SAM yields more robust predictions and effectively handles challenging categories where TP-SIS completely fails, such as GR and UP in EndoVis2017.

Figure 5 showcases a visual comparison of predicted masks by different methods, highlighting that SP-SAM clearly outperforms existing SAM-based methods in segmentation quality. Notably, SP-SAM outperforms Surgi-

calSAM, which tends to misidentify instrument categories (Fig. 5(a)), predict incomplete masks with missed critical parts like instrument tips (Fig. 5(b)), and generate rugged edges (Fig. 5(c) and (d)). Owing to the part-to-whole collaborative prompting mechanism, SP-SAM precisely captures fine-grained details such as edges and challenging areas. This precision, especially in identifying edges and tips, is crucial for ensuring safety in surgical settings.

#### 4.4. Ablation Studies

**Effectiveness of Key Components.** We conduct ablation studies on EndoVis2018 to investigate the effect of the proposed Collaborative Prompts, Part-to-Whole Selective Fusion, and Hierarchical Decoding. The results are reported in Table 3. The first row presents the baseline model which

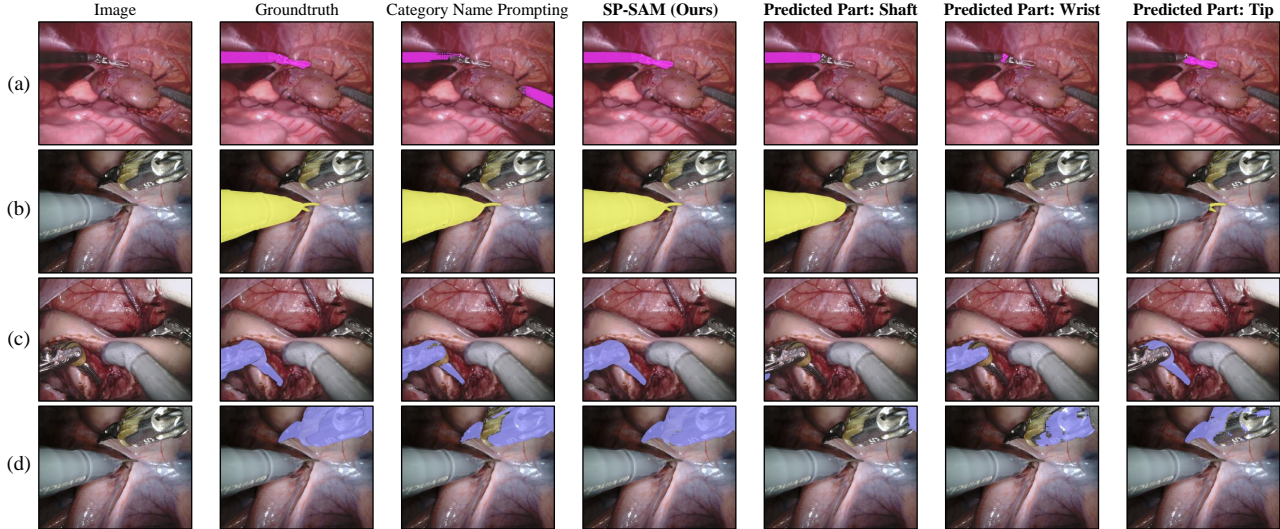


Figure 6. Visual comparison of the collaborative prompting in our SP-SAM and category name prompting.

Collab. Prompts	Part-to-Whole Fusion		Hier. Decod.	Challenge IoU	mc IoU
	Category Att.	Image Att.			
				81.08	61.14
✓				81.90	62.23
✓			✓	82.36	61.26
✓	✓		✓	82.64	63.24
✓		✓	✓	82.98	65.37
✓	✓	✓	✓	<b>84.24</b>	<b>65.71</b>

Table 3. Ablation study on the key components of SP-SAM.

uses only category name prompts. This is progressively augmented with our proposed modules. In general, it can be seen that each module individually enhances the Challenge IoU and mc IoU scores with the most significant improvements observed when all modules are integrated. In particular, after incorporating collaborative prompts (2<sup>nd</sup> row), adding Hierarchical Decoding (3<sup>rd</sup> row) shows a marginal improvement in Challenge IoU and a decrease in mc IoU. This confirms that employing surgical part labels as auxiliary signals in a straightforward multi-task learning manner does not yield substantial enhancements. The real breakthrough comes with the proposed Part-to-Whole Selective Fusion in conjunction with Hierarchical Decoding (4<sup>th</sup> - 6<sup>th</sup> rows), unlocking the full potential. A visual comparison of SP-SAM with the baseline of category name prompting is presented in Fig. 6. Prompting without part information results in a substantial loss of details in the predicted masks. In contrast, SP-SAM excels in recognising all instrument parts, particularly with intricate elements like tips (Fig. 6(a) and (b)) and areas with varying materials (Fig. 6(c) and (d)).

**Impact of the Number of Tokens.** We further examine the impact of the number of sparse tokens ( $n$ ). The results in Table 4 indicate that SP-SAM is robust to the number of tokens. The highest Challenge IoU and mc IoU scores are

Number of Tokens	Challenge IoU	mc IoU
1	83.75	65.13
2	<b>84.24</b>	65.71
4	82.63	64.76
8	83.05	<b>66.10</b>

Table 4. Influence of the number of sparse tokens in SP-SAM.

achieved with 2 and 8 tokens, respectively. We set  $n = 2$  by default for simplicity.

## 5. Conclusion

In this paper, we present SP-SAM, an efficient-tuning approach of SAM for text promptable surgical instrument segmentation. It leverages a part-to-whole collaborative prompting mechanism to address the challenge of complex structures and fine-grained patterns in surgical instruments. Specifically, collaborative prompts are devised to represent surgical instruments at both part and whole levels. Moreover, the proposed Cross-Modal Prompt Encoder, Part-to-Whole Selective Fusion, and Hierarchical Decoding modules learn discriminative representations of instrument parts and selectively assemble them for accurate instrument segmentation. Experiments on both EndoVis2018 and EndoVis2017 datasets demonstrate that SP-SAM outperforms representative specialist models and efficient-tuning methods. Our method demonstrates the great potential of efficiently adapting foundation models for domain-specific tasks and offers valuable insights into the segmentation of challenging targets. In the future, our method can be extended by exploring other forms of text prompts, incorporating temporal cues, and tackling background targets such as human tissues.

## References

- [1] Max Allan, Alex Shvets, Thomas Kurmann, Zichen Zhang, Rahul Duggal, Yun-Hsuan Su, Nicola Rieke, Iro Laina, Niveditha Kalavakonda, Sebastian Bodenstedt, et al. 2017 robotic instrument segmentation challenge. *arXiv preprint arXiv:1902.06426*, 2019. [5](#)
- [2] Max Allan, Satoshi Kondo, Sebastian Bodenstedt, Stefan Leger, Rahim Kadkhodamohammadi, Imanol Luengo, Felix Fuentes, Evangello Flouty, Ahmed Mohammed, Marius Pedersen, et al. 2018 robotic scene segmentation challenge. *arXiv preprint arXiv:2001.11190*, 2020. [5](#)
- [3] Nicolás Ayobi, Alejandra Pérez-Rondón, Santiago Rodríguez, and Pablo Arbeláez. MATIS: Masked-attention transformers for surgical instrument segmentation. In *ISBI*, pages 1–5, 2023. [2](#), [5](#), [6](#), [7](#)
- [4] Jose Daniel Azofeifa, Julieta Noguez, Sergio Ruiz, José Martín Molina-Espinosa, Alejandra J Magana, and Bedrich Benes. Systematic review of multimodal human-computer interaction. In *Informatics*, page 13. MDPI, 2022. [2](#)
- [5] Britty Baby, Daksh Thapar, Mustafa Chasmai, Tamajit Banerjee, Kunal Dargan, Ashish Suri, Subhashis Banerjee, and Chetan Arora. From forks to forceps: A new framework for instance segmentation of surgical instruments. In *WACV*, pages 6180–6190. IEEE, 2023. [2](#), [5](#), [6](#), [7](#)
- [6] Manuel Birlo, PJ Eddie Edwards, Matthew Clarkson, and Danail Stoyanov. Utility of optical see-through head mounted displays in augmented reality-assisted surgery: A systematic review. *Medical Image Analysis*, 77:102361, 2022. [2](#)
- [7] Christopher Cao and Robert J Cerfolio. Virtual or augmented reality to enhance surgical education and surgical planning. *Thoracic Surgery Clinics*, 29(3):329–337, 2019. [1](#)
- [8] Tianrun Chen, Lanyun Zhu, Chaotao Deng, Runlong Cao, Yan Wang, Shangzhan Zhang, Zejian Li, Lingyun Sun, Ying Zang, and Papa Mao. SAM-adapter: Adapting segment anything in underperformed scenes. In *ICCV*, pages 3367–3375, 2023. [3](#)
- [9] Bowen Cheng, Ishan Misra, Alexander G Schwing, Alexander Kirillov, and Rohit Girdhar. Masked-attention mask transformer for universal image segmentation. In *CVPR*, pages 1290–1299, 2022. [2](#), [6](#), [7](#)
- [10] Dongjie Cheng, Ziyuan Qin, Zekun Jiang, Shaoting Zhang, Qicheng Lao, and Kang Li. SAM on medical images: A comprehensive study on three prompt modes. *arXiv preprint arXiv:2305.00035*, 2023. [3](#)
- [11] Ruining Deng, Can Cui, Quan Liu, Tianyuan Yao, Lucas Walker Remedios, Shunxing Bao, Bennett A Landman, Yucheng Tang, Lee E Wheless, Lori A Coburn, et al. Segment anything model (SAM) for digital pathology: Assess zero-shot segmentation on whole slide imaging. In *Medical Imaging with Deep Learning, short paper track*, 2023. [3](#)
- [12] Henghui Ding, Chang Liu, Suchen Wang, and Xudong Jiang. Vision-language transformer and query generation for referring segmentation. In *ICCV*, pages 16321–16330, 2021. [3](#)
- [13] Alexey Dosovitskiy, Lucas Beyer, Alexander Kolesnikov, Dirk Weissenborn, Xiaohua Zhai, Thomas Unterthiner, Mostafa Dehghani, Matthias Minderer, Georg Heigold, Sylvain Gelly, et al. An image is worth 16x16 words: transformers for image recognition at scale. In *ICLR*, 2020. [5](#)
- [14] Guang Feng, Zhiwei Hu, Lihe Zhang, and Huchuan Lu. Encoder fusion network with co-attention embedding for referring image segmentation. In *CVPR*, pages 15506–15515, 2021. [3](#)
- [15] Cristina González, Laura Bravo-Sánchez, and Pablo Arbeláez. ISINet: an instance-based approach for surgical instrument segmentation. In *MICCAI*, pages 595–605. Springer, 2020. [2](#), [5](#), [6](#), [7](#)
- [16] Kaiming He, Georgia Gkioxari, Piotr Dollár, and Ross Girshick. Mask r-cnn. In *ICCV*, pages 2961–2969, 2017. [2](#)
- [17] Sheng He, Rina Bao, Jingpeng Li, Jeffrey Stout, Atle Bjornerud, P Ellen Grant, and Yangming Ou. Computer-vision benchmark segment-anything model (SAM) in medical images: Accuracy in 12 datasets. *arXiv preprint arXiv:2304.09324*, 2023. [3](#)
- [18] Ronghang Hu, Marcus Rohrbach, and Trevor Darrell. Segmentation from natural language expressions. In *ECCV*, pages 108–124. Springer, 2016. [3](#)
- [19] Yuhao Huang, Xin Yang, Lian Liu, Han Zhou, Ao Chang, Xinrui Zhou, Rusi Chen, Junxuan Yu, Jiongquan Chen, Chaoyu Chen, et al. Segment anything model for medical images? *arXiv preprint arXiv:2304.14660*, 2023. [3](#)
- [20] Yueming Jin, Keyun Cheng, Qi Dou, and Pheng-Ann Heng. Incorporating temporal prior from motion flow for instrument segmentation in minimally invasive surgery video. In *MICCAI*, pages 440–448. Springer, 2019. [2](#), [6](#), [7](#)
- [21] Namyup Kim, Dongwon Kim, Cuiling Lan, Wenjun Zeng, and Suha Kwak. ReSTR: Convolution-free referring image segmentation using transformers. In *CVPR*, pages 18145–18154, 2022. [3](#)
- [22] Alexander Kirillov, Eric Mintun, Nikhila Ravi, Hanzi Mao, Chloe Rolland, Laura Gustafson, Tete Xiao, Spencer Whitehead, Alexander C. Berg, Wan-Yen Lo, Piotr Dollar, and Ross Girshick. Segment anything. In *ICCV*, pages 4015–4026, 2023. [2](#), [3](#), [5](#)
- [23] Ruiyu Li, Kaican Li, Yi-Chun Kuo, Michelle Shu, Xiaojuan Qi, Xiaoyong Shen, and Jiaya Jia. Referring image segmentation via recurrent refinement networks. In *CVPR*, pages 5745–5753, 2018. [3](#)
- [24] Daochang Liu, Qiyue Li, Tingting Jiang, Yizhou Wang, Rulin Miao, Fei Shan, and Ziyu Li. Towards unified surgical skill assessment. In *CVPR*, pages 9522–9531, 2021. [1](#)
- [25] Timo Lüddecke and Alexander Ecker. Image segmentation using text and image prompts. In *CVPR*, pages 7086–7096, 2022. [3](#)
- [26] Jun Ma and Bo Wang. Segment anything in medical images. *arXiv preprint arXiv:2304.12306*, 2023. [3](#)
- [27] Maciej A Mazurowski, Haoyu Dong, Hanxue Gu, Jichen Yang, Nicholas Konz, and Yixin Zhang. Segment anything model for medical image analysis: an experimental study. *Medical Image Analysis*, page 102918, 2023. [3](#)
- [28] Fausto Milletari, Nassir Navab, and Seyed-Ahmad Ahmadi. V-Net: Fully convolutional neural networks for volumetric

- medical image segmentation. In *3DV*, pages 565–571. IEEE, 2016. 5
- [29] Zhen-Liang Ni, Gui-Bin Bian, Guan-An Wang, Xiao-Hu Zhou, Zeng-Guang Hou, Hua-Bin Chen, and Xiao-Liang Xie. Pyramid attention aggregation network for semantic segmentation of surgical instruments. In *AAAI*, pages 11782–11790, 2020. 2
- [30] Alec Radford, Jong Wook Kim, Chris Hallacy, Aditya Ramesh, Gabriel Goh, Sandhini Agarwal, Girish Sastry, Amanda Askell, Pamela Mishkin, Jack Clark, et al. Learning transferable visual models from natural language supervision. In *ICML*, pages 8748–8763. PMLR, 2021. 2, 3
- [31] Hengcan Shi, Hongliang Li, Fanman Meng, and Qingbo Wu. Key-word-aware network for referring expression image segmentation. In *ECCV*, pages 38–54, 2018. 3
- [32] Alexey A Shvets, Alexander Rakhlin, Alexandr A Kalinin, and Vladimir I Iglovikov. Automatic instrument segmentation in robot-assisted surgery using deep learning. In *ICMLA*, pages 624–628. IEEE, 2018. 2, 5, 6, 7
- [33] Tassilo Wald, Saikat Roy, Gregor Koehler, Nico Disch, Maximilian Rouven Rokuss, Julius Holzschuh, David Zimmerer, and Klaus Maier-Hein. SAM. MD: Zero-shot medical image segmentation capabilities of the segment anything model. In *Medical Imaging with Deep Learning, short paper track*, 2023. 3
- [34] An Wang, Mobarakol Islam, Mengya Xu, Yang Zhang, and Hongliang Ren. SAM meets robotic surgery: An empirical study on generalization, robustness and adaptation. *arXiv preprint arXiv:2308.07156*, 2023. 3
- [35] Zhaoqing Wang, Yu Lu, Qiang Li, Xunqiang Tao, Yandong Guo, Mingming Gong, and Tongliang Liu. CRIS: Clip-driven referring image segmentation. In *CVPR*, pages 11686–11695, 2022. 3
- [36] Jianzong Wu, Xiangtai Li, Xia Li, Henghui Ding, Yunhai Tong, and Dacheng Tao. Towards robust referring image segmentation. *arXiv preprint arXiv:2209.09554*, 2022. 3
- [37] Junde Wu, Rao Fu, Huihui Fang, Yuanpei Liu, Zhaowei Wang, Yanwu Xu, Yueming Jin, and Tal Arbel. Medical SAM adapter: Adapting segment anything model for medical image segmentation. *arXiv preprint arXiv:2304.12620*, 2023. 3
- [38] Jinyu Yang, Mingqi Gao, Zhe Li, Shang Gao, Fangjing Wang, and Feng Zheng. Track anything: Segment anything meets videos. *arXiv preprint arXiv:2304.11968*, 2023. 6, 7
- [39] Linjie Yang, Yuchen Fan, and Ning Xu. Video instance segmentation. In *ICCV*, pages 5188–5197, 2019. 6
- [40] Zhao Yang, Jiaqi Wang, Yansong Tang, Kai Chen, Hengshuang Zhao, and Philip HS Torr. Lavt: Language-aware vision transformer for referring image segmentation. In *CVPR*, pages 18155–18165, 2022. 3
- [41] Linwei Ye, Mrigank Rochan, Zhi Liu, and Yang Wang. Cross-modal self-attention network for referring image segmentation. In *CVPR*, pages 10502–10511, 2019. 3
- [42] Wenxi Yue, Jing Zhang, Kun Hu, Yong Xia, Jiebo Luo, and Zhiyong Wang. Surgicalsam: Efficient class promptable surgical instrument segmentation. *arXiv preprint arXiv:2308.08746*, 2023. 2, 3, 6, 7
- [43] Dongqing Zang, Gui-Bin Bian, Yunlai Wang, and Zhen Li. An extremely fast and precise convolutional neural network for recognition and localization of cataract surgical tools. In *MICCAI*, pages 56–64. Springer, 2019. 1
- [44] Kaidong Zhang and Dong Liu. Customized segment anything model for medical image segmentation. *arXiv preprint arXiv:2304.13785*, 2023. 3
- [45] Renrui Zhang, Zhengkai Jiang, Ziyu Guo, Shilin Yan, Junting Pan, Hao Dong, Peng Gao, and Hongsheng Li. Personalize segment anything model with one shot. *arXiv preprint arXiv:2305.03048*, 2023. 6, 7
- [46] Zixu Zhao, Yueming Jin, Xiaojie Gao, Qi Dou, and Pheng-Ann Heng. Learning motion flows for semi-supervised instrument segmentation from robotic surgical video. In *MICCAI*, pages 679–689. Springer, 2020. 2, 6, 7
- [47] Zixu Zhao, Yueming Jin, and Pheng-Ann Heng. TraSeTr: track-to-segment transformer with contrastive query for instance-level instrument segmentation in robotic surgery. In *ICRA*, pages 11186–11193. IEEE, 2022. 2, 6, 7
- [48] Zijian Zhou, Oluwatosin Alabi, Meng Wei, Tom Vercauteren, and Miaoqing Shi. Text promptable surgical instrument segmentation with vision-language models. In *NeurIPS*, 2023. 2, 6, 7